THE ASTRONOMICAL JOURNAL VOLUME 92, NUMBER 2 FEBRUARY 1987

EVIDENCE FOR LARGE-SCALE WINDS FROM STARBURST GALAXIES. II. AN OPTICAL INVESTIGATION OF POWERFUL FAR-INFRARED GALAXIES

TIMOTHY M. HECKMAN[a),b)] AND LEE ARMUS[a)]
Astronomy Program, University of Maryland, College Park, Maryland 20742

GEORGE K. MILEY[a),c)]
Space Telescope Science Institute, Homewood Campus, The Johns Hopkins University, Baltimore, Maryland 21218
Received 11 July 1986; revised 10 October 1986

ABSTRACT

We discuss our program of long-slit spectroscopy and narrowband (Hα) imaging of a sample of powerful ($\sim 10^{12}\ L_\odot$) far-infrared galaxies (FIRGs). The sample was selected so that the mid/far infrared spectral energy distributions resembled those of the prototypes Arp 220 and NGC 6240 ("tepid" FIRGs). The principal new observational results are as follows: (1) As a class, the emission-line spectra of tepid FIRGs are most similar to LINERs, but about half are intermediate between LINERs and low-excitation H II regions. The sample as a whole bears a strong spectroscopic resemblance to the well-known M82 filaments. (2) Huge (10^4–10^5 pc) and morphologically spectacular (multiple filaments, loops, or bubbles) emission-line nebulae resembling the M82 filament system are associated with both NGC 6240 and Arp 220. Spatially extended ($\gtrsim 10$ kpc) nebulae are also evident in some of the much more distant FIRGs in our sample. We propose that the model considered by Chevalier and Clegg (1985) and McCarthy, Heckman, and van Breugel (1987) for M82 be generalized to encompass powerful far-infrared galaxies as a class: a starburst-driven bipolar superwind (with a mass flux 10–100 $M_\odot$/yr and kinetic energy flux of 10^{44}–10^{45} erg s^{-1}) escapes along the rotation axis of a circumnuclear disk and then sweeps up and shock heats gaseous "tidal debris" around the galaxy, producing optical line emission and possibly x rays.

I. INTRODUCTION

The most extraordinary extragalactic discovery made by *IRAS* is the existence of galaxies with far-infrared luminosities $L_{\rm IR} \sim 10^{11}$–$10^{12}\ L_\odot$ and ratios of infrared to blue luminosity of $L_{\rm IR}/L_B \sim 10$–100 (e.g., Soifer *et al.* 1984). We will term these far-infrared galaxies "FIRGs," and define them to have $L_{\rm IR}/L_B > 10$. Ground-based optical, infrared, and radio investigations of the prototypical class members NGC 3690, Mrk 231, NGC 6240, and Arp 220 (e.g., Gehrz *et al.* 1983; Cutri *et al.* 1984; Rieke *et al.* 1985) strongly suggest that the circumnuclear ($r \lesssim 1$ kpc) regions of FIRGs are the sites of tremendous "bursts" of star formation. In essence, these galaxies may be similar to the nearby well-studied galaxies M82 and NGC 253 (Rieke *et al.* 1980), but with a star-formation rate that is tens of times larger. However, evidence that a compact active nucleus is present and may play an important energetic role in some of the FIRGs has also been uncovered (cf. the above references and Norris *et al.* 1985; Depoy *et al.* 1986).

The sample of well-studied, powerful FIRGs is still small, so that little can be said concerning the properties of such galaxies as a class. Several important questions remain to be answered, such as:

(1) What is the ultimate source of the enormous energies involved?

(2) How is the raw energy generated in the circumnuclear region subsequently reprocessed into the observed infrared, optical, and radio emission?

(3) Are FIRGs related to other classes of active galaxies, such as Seyfert galaxies, radio galaxies, and QSOs, and, if so, how?

(4) What is the impact of this prodigious energy release on the rest of the galaxy?

The answers to such questions are likely to prove fascinating in their own right. They may also offer us unique insights into the formation of stars and galaxies under the extreme conditions that prevailed in the early universe.

To better understand the phenomenon of FIRGs, we have identified a large sample of optically faint *IRAS* galaxies all having the same distinctive far-infrared spectral shape as the above prototypes. In the present paper, we primarily discuss the results of long-slit spectroscopy of 20 such galaxies, and present deep narrowband images of the prototypes Arp 220 and NGC 6240. We describe our sample-selection criteria in Sec. II, our observations in Sec. III, our results in Sec. IV, and our interpretation and its implications in Sec. V.

II. SAMPLE SELECTION

We believe that we have uncovered a highly efficient technique for locating additional FIRGs. It is similar to that used by DeGrijp *et al.* (1985) to discover several hundred new Seyferts, namely use of an *IRAS* color-color diagram. We noticed that the prototype powerful FIRGs occurred in a well-defined part of the infrared color-color diagram which is sparsely populated by other galaxies (Fig. 1). Specifically, we have generated a list of 298 objects from the *IRAS Point Source Catalog* meeting the following spectral shape criteria:

(1) $\alpha_{25\mu}^{60\mu} < -1.5$,

(2) $\alpha_{60\mu}^{100\mu} > -0.5$,

[a)] Visiting Astronomers at the Kitt Peak National Observatory and Cerro Tololo Inter-American Observatory of the National Optical Astronomy Observatories, operated by AURA, Inc., under contract with the NSF.
[b)] Alfred P. Sloan Foundation Fellow.
[c)] Affiliated with the Astrophysics Division, Space Science Department of the European Space Agency. On leave from Leiden Observatory.

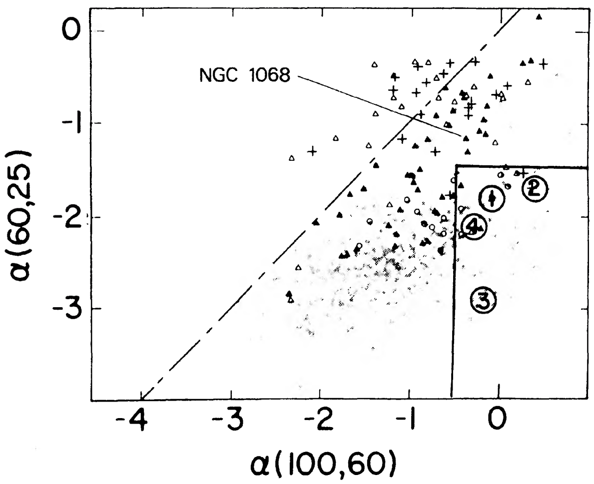

FIG. 1. Mid-to-far-infrared color-color plot for galaxies with strong nuclear emission lines. The spectral indexes are defined in the text. In all figures, Seyfert 1 galaxies are denoted by light triangles, Seyfert 2 galaxies are denoted by dark triangles, galaxies with nuclear H II regions by circles, and QSOs by crosses. The shaded region denotes the colors of nonactive spirals of an IR-defined sample of galaxies (adapted from Miley, Neugebauer, and Soifer 1985). The region selected for our investigation is at the lower right bounded by the solid lines. The prototypical powerful far-infrared galaxies NGC 3690, Mrk 231, Arp 220, and NGC 6240 are denoted by the circled numbers 1 through 4, respectively.

where

$$\alpha_1^2 \equiv \frac{\log [S_\nu(\lambda_1)] - \log [S_\nu(\lambda_2)]}{\log [\lambda_2] - \log[\lambda_1]},$$

and where the S_ν at 25, 60, and 100 μ are taken (uncorrected for spectral bandpass shape) directly from the *IRAS Point Source Catalog.*

In Fig. 1 we plot an infrared two-color diagram ($\alpha_{25\,\mu}^{60\,\mu}$ vs $\alpha_{60\,\mu}^{100\,\mu}$) for a large sample of Seyfert galaxies, QSOs, Markarian starburst galaxies, and normal galaxies. The locations of the prototypical members of the class of powerful FIRGs (Mrk 231, NGC 3690, NGC 6240, and Arp 220) are also indicated.

The mid/far infrared properties of objects meeting our selection criteria (steeply rising continuum out to $\lambda = 60\,\mu$ with a subsequent flattening or decline at longer wavelengths) suggest a model in which the infrared emission is generated by thermal radiation from dust grains that have higher characteristic temperatures than in normal galaxies (de Jong *et al.* 1984). We will term such far-infrared spectra "tepid" to differentiate them from both the cooler spectra of normal galaxies and the warmer spectra of Seyfert galaxies (e.g., DeGrijp *et al.* 1985). An inverse correlation for galaxies between the infrared luminosity and the spectral slope between $\lambda = 60$ and $100\,\mu$ has been previously noted by others as well (e.g., de Jong *et al.* 1984; Miley, Neugebauer, and Soifer 1986; Rieke and Lebofsky 1986).

We have systematically attempted to identify the 298 *IRAS* sources selected this way using the Palomar Observatory Sky Survey and ESO/SRC Southern Sky Survey. The full set of positions, infrared fluxes, etc., will be published elsewhere, together with a detailed analysis of our broadband multicolor images and spectroscopic data (Armus, Heckman, and Miley, in preparation, hereafter referred to as AHM).

For the sample of 298 sources, we selected a subsample of objects for subsequent optical observations. These objects were chosen on the basis of both accessibility and optical faintness (the latter being designed to focus our attention first on those objects with the most extreme properties, namely high L_{IR}/L_B and L_{IR}).

III. OBSERVATIONS AND DATA REDUCTION

Our observations are summarized in Table I. Standard calibration and analysis techniques were employed using the NOAO's IRAF package at KPNO and at STScI, and the NRAO's AIPS package at the STScI. All the imaging data have been flux calibrated using observations of KPNO IIDS or Landolt (1973, 1983) standard stars, except for the KPNO February 86 data (obtained through highly variable cloud cover). Further details concerning the observations, data reduction, and data analysis can be found in the footnotes to Tables II and III, and in AHM.

IV. RESULTS

a) Optical Imaging

We will present (and discuss in detail) the results of our broadband imaging survey in AHM. Here we remark merely that at least half of the identified *IRAS* galaxies we have imaged are markedly peculiar in optical morphology (exhibiting tails, plumes, non-elliptical isophotes, etc.). The strong connection between galaxy morphological peculiarity (interpreted as indicative of galaxy collisions or mergers) and strong far-infrared emission has been noted previously by several authors (e.g., Soifer *et al.* 1984; Joseph *et al.* 1984).

More germane to the present paper are the narrowband (Hα plus [N II]) images of the prototypical tepid FIRGs Arp 220 and NGC 6240 (Figs. 2 and 3 [Plates 5 and 6], respectively). Examination of these figures reveals the following:

TABLE I. Observations.

(1) Telescope	(2) Instrument	(3) Field of view	(4) Pixel size	(5) Spectral range	(6) Dates	(7) Number of galaxies
KPNO 4 m	Cryogenic camera	3.2×233 arcsec	0.8 arcsec×4.3 Å	4500–8000 Å	2/86	4
KPNO 4 m	Prime-focus CCD	234×234 arcsec	0.6×0.6 arcsec	*R*, redshifted Hα	4/86	9
KPNO 0.9 m	CCD direct	317×317 arcsec	0.8×0.8 arcsec	*B,R*	10/85; 2/86	32
CTIO 4 m	CCD Cass. spectrometer	1.5×284 arcsec	0.73 arcsec×5.7 Å	5495–8775 Å and 4925–8195 Å	12/85	16
CTIO 1.5 m	CCD direct	230×154 arcsec	0.4×0.4 arcsec	*B,R*	12/85	13

TABLE II. Properties of emission-line nebulae.

(1) Galaxy	(2) Distance	(3) Total Size	(4) $L_{H\alpha[N\,II]}$	(5) Feature Size	(6) Surf. Bright	(7) L_{IR}	(8) L_x
M82	3	$>2.6\times>1.3$	0.5	0.1–1	3–400	1.5	~2
Arp 220	72	24×10	1.1	≤1–10	0.3–7	80	~10
NGC 6240	98	60×50	18.2	≤1–20	0.3–120	33	?

Notes to TABLE II

Col. 2. The distance (in Mpc) assumed for each galaxy.
Col. 3. The overall dimensions (in kpc) of the emission-line nebula to an Hα [N II] surface-brightness level of $\sim3\times10^{-17}$ erg cm^{-2} s^{-1} arcsec^{-2} in the filaments/loops. For M82, the nebula extends beyond the boundaries of our CCD frame, and is 2.6×1.3 kpc in size at $\sim3\times10^{-16}$ erg cm^{-2} s^{-1} arcsec^{-2} in Hα[N II].
Col. 4. The total Hα plus [N II] λλ 6548,6584 luminosity in 10^{41} erg s^{-1}, with no correction made for dust extinction. For M82, the quoted luminosity refers to the area listed in Col. 3 (see MHvB for details).
Col. 5. The size range (in kpc) of typical individually prominent loops and filaments.
Col. 6. The range in surface brightness (Hα plus [N II]) of typical prominent loops and filaments (in 10^{-16} erg cm^{-2} s^{-1} arcsec^{-2}).
Col. 7. The far-infrared "luminosity" (in units of 10^{10} $L_\odot$) constructed using the far-infrared flux ("FIR") as defined in *Cataloged Galaxies and Quasars Observed in the IRAS Survey* (Lonsdale *et al.* 1985) and the distance listed in Col. 2 of this table. This is effectively the total luminosity between the wavelengths of 42.5 and 122.5 μ (Earth rest frame).
Col. 8. The 0.2–4 keV x-ray luminosity in units of 10^{40} erg s^{-1} taken from Watson, Stanger, and Griffiths (1984) for M82 and from R. Mushotzky (private communication) for Arp 220. NGC 6240 was not observed with the *Einstein* Observatory.

(1) Both galaxies have large and morphologically spectacular emission-line nebulae.

(2) The nebula associated with Arp 220 (Fig. 2) is some 24×10 kpc in total extent, while the NGC 6240 nebula (Fig. 3) is even larger ($\sim60\times50$ kpc). In both cases these sizes are measured down to a level of surface brightness of $\sim3\times10^{-17}$ erg cm^{-2} s^{-1} arcsec^{-2} in the sum of the Hα + [N II] λλ 6548, 6584 lines.

(3) The nebula associated with Arp 220 is relatively faint, with a total Hα + [N II] luminosity of $\sim10^{41}$ erg s^{-1}. The NGC 6240 nebula is considerably more luminous (1.7×10^{42} erg s^{-1}). Since both galaxies are dusty, the intrinsic luminosities could be significantly greater.

(4) The Arp 220 nebula is morphologically simple: at levels of surface brightness $\lesssim4\times10^{-17}$ erg cm^{-2} s^{-1} arcsec^{-2} it is strongly bipolar in form (oriented in a P.A. ~105°), consisting of two large loops or bubbles (one on either side of the nucleus). Each bubble is ~10 kpc in diameter. At higher levels of surface brightness ($\gtrsim10^{-16}$ erg cm^{-2} s^{-1} arcsec^{-2}), the inner part of the nebula is oriented in P.A. ≃ 135°, nearly perpendicular to the central dust lane running in P.A. ~40° (see Fig. 2b). We note that the orien-

TABLE III. Optical spectroscopic properties.

(1) Galaxy	(2) z	(3) $E_{H\alpha}$	(4) $F_{H\alpha}$	(5) $L_{H\alpha}$	(6) [O III]/Hβ	(7) [O I]/Hα	(8) [N II]/Hα	(9) [S II]/Hα	(10) L_{IR}
00182 − 7112	0.327	—	(0.80)	(2.2)	0.83:				400
00188 − 0856	0.125	15	2.2	0.75		≤ − 1.0	0.13		107
01003 − 2238	0.118	160	8.5	2.6		− 1.20	− 0.70	− 0.76	69
01217 + 0122	0.138	110	13.5	5.7	1.03	− 0.87	− 0.11		102
02021 − 2104	0.116	10	0.83	0.24		≤ − 0.70	0.08	− 0.22:	46
05100 − 2425	0.034	52	24	0.55	0.38	− 1.2	− 0.80	− 0.56	11
05447 − 2114	0.040	46	14	0.45	0.2:	− 1.45:	− 0.18	− 0.38	5.4
06361 − 6217	0.160	37	2.1	1.2	0.1:	− 0.85:	− 0.25	0.0	108
07205 + 7842	0.087	46*	23	3.6	0.6	− 1.01	− 0.15	− 0.53	25
08539 − 1208	0.038	108	32	0.93	0.14	− 1.41	− 0.43	− 0.54	60
09143 + 0939	0.047	44	12	0.54	0.09	− 1.04	− 0.18	− 0.33	17
09168 + 0623	0.083	229	32	4.6		− 1.56:	− 0.66	− 0.63	23
09192 + 2124	0.078	81*	14	1.8	0.25	− 1.21	− 0.40	− 0.53	36
10485 − 1447	0.133	20	1.1	0.43		< − 0.7	− 0.11:		75
10502 − 1843	0.054	53	7.6	0.45		− 1.14:	− 0.14	− 0.36	28
11095 − 0238	0.106	117	8.6	2.1	0.09	− 0.84	− 0.21	− 0.30	79
11119 + 3257	0.187	197*	63	51	0.14	< − 1.50	< − 0.50		142
11120 − 2919	0.030	17	6.9	0.12		− 1.00:	− 0.03	− 0.39	3.4
12018 + 1941	0.169	24	1.8	1.2	>0	− 0.85	− 0.05	− 0.21	116
15225 + 2350	0.138	57*	5.3	2.2	0.22:	− 1.13:	− 0.35	− 0.68:	65

Notes to TABLE III

Col. 3. The rest-frame equivalent width of the Hα emission line in our spectra (typical aperture size was 1.5×4.4 arcsec, except where denoted by an asterisk, where the aperture size was 3.2×4.0 arcsec).
Col. 4. Estimated flux in the Hα line (in 10^{15} erg cm^{-2} s^{-1}) through the aperture defined above. The spectra were not flux calibrated, and the quoted $F_{H\alpha}$ comes from the measured continuum flux density from our calibrated direct images (through the appropriate aperture size). For 00182, the Hα line fell redward of the spectral bandpass and the quoted $F_{H\alpha}$ is actually the [O III] λ 5007 flux. We estimate that these derived fluxes are uncertain by a factor of about 2.
Col. 5. The Hα luminosity (in 10^{41} erg s^{-1}) calculated using the Hα flux from Col. 3 and the measured redshift (Col. 2) for $H_0=75$ km s^{-1}/Mpc and $q_0=0$. *No correction for dust extinction has been applied.* The luminosities are uncertain by a factor of about 2 (see note above).
Cols. 6–9. The logarithm of the ratio of detected photons for various pairs of emission lines. Note that "[O III]" means [O III] λ 5007, "[O I]" means [O I] λ 6300, "[N II]" means [N II] λ 6584, and "[S II]" means [S II λλ 6717, 6731. A blank implies that the ratio could not be determined (neither line reliably detected or one or both lines were outside the spectral range covered). Uncertainties are typically ≲ 0.1, except where indicated by a colon (± 0.2 dex). None of the reported line ratios have been corrected for the effects of absorption lines in the stellar continuum. The [O III]/Hβ will be most affected by strong stellar Balmer absorption lines and so the true [O III]/Hβ ratio *could* be significantly smaller than quoted.
Col. 10. The far-infrared luminosity in units of 10^{10} $L_\odot$, as defined in the notes to Table II for $H_0=75$ km s^{-1}/Mpc and $q_0=0$.

tation of the double bubble system is the same as that of the much smaller ($2'' = 700$ pc) nonthermal radio source and OH "megamaser" region (Norris *et al.* 1985).

(5) The NGC 6240 nebula is much more complex in morphology, exhibiting long, radial filaments and several loops or bubbles with sizes varying from ~ 2 to ~ 20 kpc. At high levels of surface brightness ($\gtrsim 10^{-15}$ erg cm^{-2} s^{-1} arcsec^{-2}), the inner part of the nebula is elongated in P.A. $\simeq 105°$, roughly orthogonal to the bright main body of the galaxy itself (major axis in P.A. $\simeq 25°$).

(6) The nebulae look similar to the filament system associated with the infrared galaxy M82 (see McCarthy, Heckman, and van Breugel 1987, hereafter referred to as MHvB).

b) Optical Spectroscopy

1) Classification

The principal results of our optical spectroscopy of 20 galaxies are summarized in Table III, and several representative examples of the spectra are displayed in Fig. 4. One of our primary goals was to understand the excitation source for the optical emission-line gas, as this may provide insight into the energy source for the infrared emission. Accordingly, we have attempted to classify our emission-line spectra into the major categories of known nuclear emission-line regions (cf. Heckman 1986): (1) Seyfert (gas that is photoionized by a high-energy continuum source); (2) LINER (gas that is shock heated or photoionized by a dilute but high-energy continuum source); and, (3) H II region (gas that is photoionized by OB stars). For the purposes of classification, we have used a technique popularized by Baldwin, Phillips, and Terlevich (1981), who plotted diagrams of various pairs of emission-line flux ratios ("BPT diagrams"); see also Veilleux and Osterbrock (1986).

Several representative BPT diagrams are displayed in Figs. 5 and 6. The locations occupied by Seyferts, LINERs, H II regions, and various theoretical models are indicated schematically, while the spectra of our *IRAS* galaxies (Table III) and of other tepid FIRGs with spectra in the literature (see Table IV) are plotted individually.

A careful inspection of Figs. 5 and 6 reveals the following:

(1) Considered as a class, about half the tepid FIRGs can be comfortably categorized as LINERs. The other half fall outside (in between) the regions occupied by LINERs and low-excitation H II regions in the various BPT diagrams. This behavior is illustrated in Figs. 5 and 6, but is evident in all the BPT diagrams that we can construct.

(2) The spectra of the emission-line filaments in M82 are

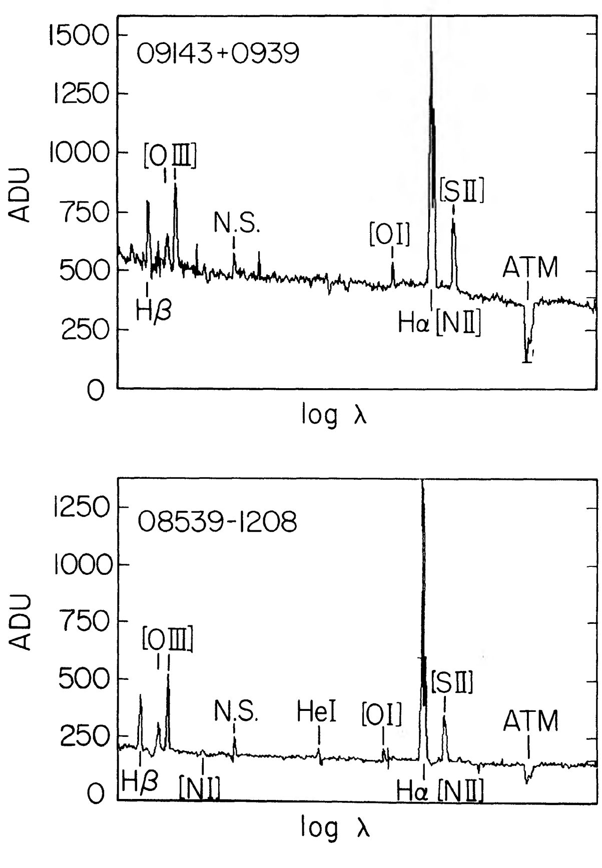

FIG. 4. Several representative emission-line spectra of galaxies from Table III. The spectra are plotted in ADU vs log λ (1 ADU $\simeq 13$ detected photons).

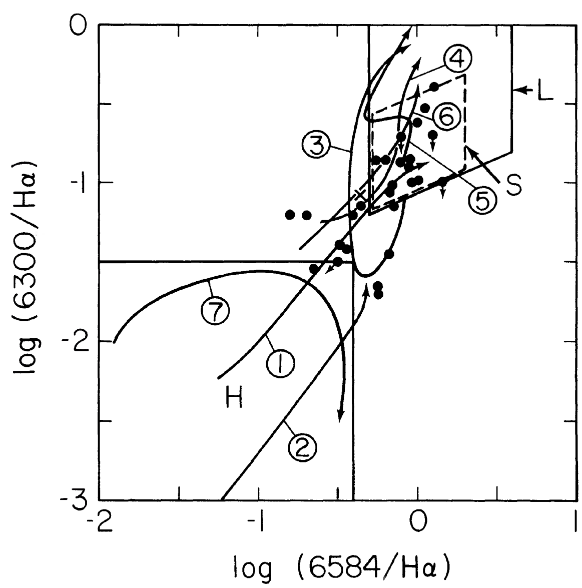

FIG. 5. The log of the ratio of the [O I] λ 6300 and Hα emission lines is plotted versus the log of the ratio of the [N II] λ 6584 and Hα emission lines. The regions occupied by H II regions ("H"), Seyfert nuclei ("S"), and LINERs ("L") are indicated by boxes. The galaxies from Tables III and IV are indicated by solid dots, while the average spectrum of the filaments in M82 (see MHvB) is indicated by a cross. The loci of various theoretical models are indicated by solid lines with arrows indicating the direction over which the models run (see below). The models are identified according to the following code: (1) H II-region models of Evans and Dopita (1985) with $T_* = 56\,000$ K and log U running from -1.5 to -3.5. (Note: U is the ratio of the ionizing photon and electron number densities in the photoionized gas). (2) Evans and Dopita H II region model with $T_* = 40\,000$ K and log U running from -1.7 to -3.5. (3) Shock models of Raymond (1979) with shock velocity running from 50 to 200 km/s (his models A through I). (4) Shock models of Shull and McKee (1979) with shock velocity running from 40 through 130 km/s (their models A through G). (5) Shock models of Binette, Dopita, and Tuohy (1985) with shock velocity running from 86 to 268 km/s. (6) Terlevich and Melnick (1985) "Warmer" models with log U running from -2 to -4. (7) McCall, Rybski, and Shields (1985) H II region models with metal abundances ranging from 0.1 through 4 times solar.

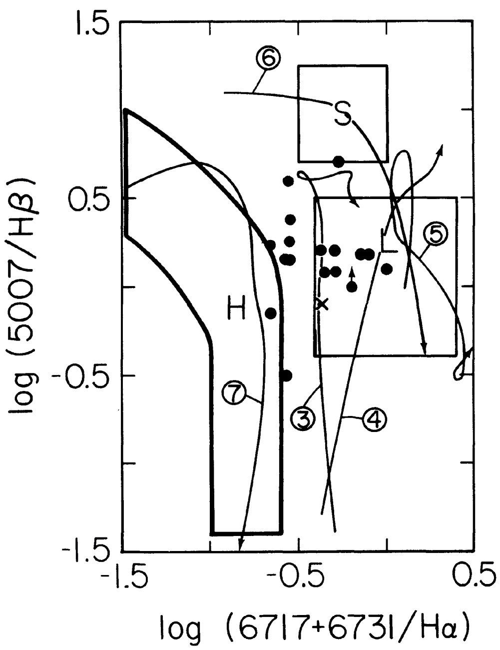

FIG. 6. The log of the ratios of the [O III] λ 5007 and Hβ emission lines are plotted against the log of the ratios of the [S II] $\lambda\lambda$ 6717, 6731 and Hα emission lines. The symbols, lines, and boxes have the same meaning as in Fig. 5.

quite similar to both the spectra of our *IRAS* galaxies and to the spectra of the Arp 220 and NGC 6240 nebulae (see Tables III and IV). This strongly suggests a physical relationship between these objects.

2) Spectroscopy of spatially extended emission-line gas

The point-spread function (along the slit) is poorly determined for our spectra and varied during our observations. This (and the large redshifts of most of our galaxies) makes it difficult to assess the fraction of galaxies in our sample that

TABLE IV. Optical spectra from the literature.

(1)	(2) [O III]/Hβ	(3) [O I]/Hα	(4) [N II]/Hα	(5) [S II]/Hα	(6) Refs.
NGC 1614	−0.15	−1.70	−0.22	−0.68	1
M82 inner	−0.50	−1.55	−0.30	−0.61	2,3
M82 outer	−0.23	−0.87	−0.26	−0.25	2
NGC 3690	0.15	−1.41	−0.47	−0.57	4,5
Mrk 273	0.70	−0.88	−0.05	−0.28	6
Arp 220 inner	0.2	−1.0	0.0	−0.3	7
Arp outer	—	−0.4	0.1	0.0	7
NGC 6240 inner	0.19	−0.61	0.00	−0.10	8,9,10
NGC 6240 outer	0.20	−0.52	0.05	−0.13	8,9,10

Notes to TABLE IV

Cols. 1–5. See Table III notes.
Col. 6. References for the emission-line ratios according to the following key:
1. A. S. Wilson, private communication.
2. McCarthy *et al.* (1986).
3. Heckman, Balick, and Crane (1980).
4. French (1980).
5. Keel (1984).
6. Koski (1978).
7. P. McCarthy, private communication.
8. Fosbury and Wall (1979).
9. Fried and Schulz (1983).
10. Heckman, unpublished data.

definitely have emission-line nebulae similar in size and brightness to the nebulae associated with M82, Arp 220, and NGC 6240. Nevertheless, several clear-cut examples of such nebulae have been uncovered (these are unambiguously extended because of a complex or asymmetric brightness distribution of line emission along the slit and/or because of a large angular size).

The following galaxies are associated with the most clearly established examples of such nebulae (see Fig. 7): 00182 − 7112 ($\sim$55 kpc in size), 09143 + 0939 ($\sim$12 kpc in size), 10502 − 1843 ($\sim$10 kpc in size), and 11120–2919 ($\sim$10 kpc in size). These sizes are measured at levels of surface brightness 10^{-16} erg cm^{-2} s^{-1} arcsec^{-2} in Hα—plus—[N II] or (for 00182 − 7112) of 4×10^{-17} erg cm^{-2} s^{-1} arcsec^{-2} in [O III] λ 5007 (see Table II for comparison).

V. DISCUSSION

a) Summary of Clues

The primary observational clues as to the nature of the tepid FIRGs can be summarized as follows:

(1) The galaxies are often highly peculiar in optical morphology, suggesting that galaxy collisions and/or mergers are occurring.

(2) Considered as a class, about half the optical emission-line spectra can be classified as LINERs and the other half appear intermediate between LINERs and low-excitation H II regions. The emission-line spectra strongly resemble the spectra of the filaments in M82 (MHvB). It is possible that the spectrum of a typical tepid FIRG is a mix of different spatially and physically distinct components (e.g., LINER nucleus surrounded by giant H II regions). However, the emission-line filaments of M82 clearly cannot be explained in this way, but instead must be the result of a special set of physical conditions. We suggest that the same applies to tepid FIRGs as a class.

(3) Two of the nearest prototypes of the class (namely NGC 6240 and Arp 220) have morphologically spectacular nebulae of ionized gas, consisting of giant loops, bubbles, filaments, and arcs arrayed over a large region (tens of kpc in size). The nebulae are morphologically and spectroscopically similar to the M82 filament system. Nebulae with similar sizes and spectra are associated with some of the more distant galaxies in our sample.

b) A Model: Superwinds from Superstarbursts

We believe that the model which some of us have explored in detail for the filament system in M82 (MHvB) can be readily applied to the class of tepid FIRGs discussed above. In particular, we propose the following scenario to account for the various observational clues summarized above:

(1) The collision or merger of two galaxies (at least one of which is rich in cold gas) leads to the accretion of a large mass of gas into a circumnuclear ($\lesssim$ few kpc) disk in one or both galaxies (e.g., Toomre and Toomre 1972).

(2) A burst of star formation (and possibly a release of energy from a compact active nucleus) is triggered in the central region of the circumnuclear molecular disk.

(3) The kinetic energy produced by the many supernovae that soon follow the initial starburst (and/or the mechanical energy that is produced by the compact active nucleus) is efficiently thermalized via high-speed gas collisions (shocks), creating a central cavity of hot (few $\times 10^8$ K) gas

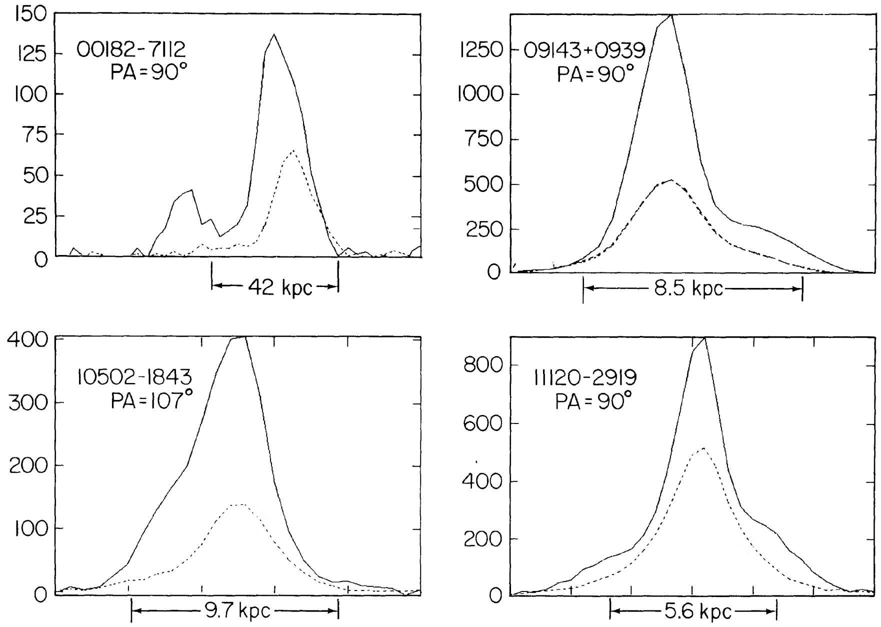

FIG. 7. Plots of the emission-line surface brightness along the spectroscopic slit for four galaxies from Table III (solid lines). The emission line used is Hα for all galaxies except 00182 − 7112 ([O III] λ 5007). The overplotted dashed lines show the surface-brightness distribution in the spectrally adjacent continuum (starlight). The vertical scales are in ADU/pixel. The bars along the horizontal axes indicate 10 arcsec, with the corresponding linear scale for $H_0 = 75$ km s^{-1} Mpc^{-1} and $q_0 = 0$ being indicated on each figure.

in the molecular disk. This hot gas then flows outward as a high-speed ($\gtrsim$ few $\times 10^3$ km s^{-1}) wind with a kinetic energy flux of $\dot{E}_{\rm wind} \sim 0.1\, L_{\rm IR}$, as described by Chevalier and Clegg (1985).

(4) The wind so produced may be bipolar in form, as the wind material preferentially escapes along the rotation axis of the circumnuclear disk of dense gas that is fueling the star formation and/or nuclear activity.

(5) As the wind flows out it collides with, shocks, and sweeps up gas clouds that are associated with the accretion process (gaseous tidal debris). Clouds with relatively low densities have high-speed (300–1000 km s^{-1}) shocks driven into them by the wind and may emit x rays. Clouds with higher densities suffer only slow shocks ($\sim 10^2$ km s^{-1}) and can produce strong optical line radiation having a spectrum similar to that observed in the nebulae (e.g., Raymond 1979; Shull and McKee 1979). The large loop-like structures of ionized gas (seen in Figs. 2 and 3 and in MHvB) may represent dense shells of rapidly cooling, swept-up material. Only a small fraction of the wind's kinetic energy need go into producing optical/near-ultraviolet emission lines: taking $\dot{E}_{\rm wind} \sim 0.1\, L_{\rm IR}$, the values for $L_{\rm H\alpha}$ and $L_{\rm IR}$ from Tables III and IV, models for shock-heated gas (e.g., Shull and McKee 1979), and modest extinction in the emission-line nebulae implies fractions in the range $\lesssim 10^{-2}$–10^{-1}. This fraction must depend in a complex way on the nature of the ambient cloud-strewn medium into which the wind flows.

(6) Ionizing radiation from the massive stars (and/or from a compact active nucleus) can also escape along the rotation axis of the circumnuclear gas disk, traveling out through the channels/nozzles formed by the bipolar wind. This dilute radiation field may (like shocks) play an important role in the ionization/heating of the optically emitting gas, possibly accounting for the intermediate location of the spectra of the *IRAS* galaxies in BPT diagrams (Figs. 5 and 6). The galaxy's aspect angle (the extent to which a distant observer sees directly down into the nucleus along the wind's flow axis) may also help to determine the nature of the observed emission-line spectrum (i.e., the relative prominence of inner, starburst-photoionized versus outer, wind-shock-heated gas). On the other hand, if the ionizing radiation from the starburst is dominated by the light of stars that are hotter than ordinary O stars (like the "Warmers" investigated by Terlevich and Melnick (1985) or the $T_* \sim 57\,000$ K stars modeled in Evans and Dopita (1985), a LINER-like spectrum can result even without shock heating (see Figs. 5 and 6 and MHvB for details, and also Heckman (1986)).

c) Alternative Models

Large (> 10 kpc) emission-line nebulae are associated with a wide variety of galaxies, and have a correspondingly wide range of interpretations. While we have argued above that the nebulae associated with FIRGs can be plausibly interpreted as visible manifestations of "superwinds," the evidence is indirect and rests largely on their similarity to the well-studied nebulae in NGC 253 and especially M82 (MHvB). We will therefore briefly evaluate other possible interpretations of the FIRG nebulae.

The class of emission-line nebulae bearing the closest resemblance to the FIRG nebulae are those associated with cooling flows of x-ray gas onto dominant galaxies in rich clusters (cf. the reviews of Fabian, Nulsen, and Canizares 1984; Sarazin 1986; and the recent paper by Hu, Cowie, and Wang 1985). Indeed, the extensive LINER-like filamentary systems around the FIRG NGC 6240 and the cooling flow/radio galaxy NGC 1275 are remarkably similar in both morphology and emission-line spectra (e.g., Kent and Sargent 1979). However, it is physically most implausible for the FIRG nebulae to be cooling flows, as there is no evidence for the vast reservoir of hot gas out of which the cool, optically emitting filaments could form. While the ratio of $L(\mathrm{x})/L(\mathrm{H}\alpha)$ is typically observed to be $\gtrsim 10^3$ in cooling-flow galaxies (as expected for gas cooling from $T \gtrsim 10^7$ K) it is only 0.1 to 1 for the FIRGs Arp 220, NGC 253, and M82 (see Table II and MHvB). The Hα fluxes for the other FIRGs in Tables III and IV are similar to those of the cooling-flow galaxies considered by Hu, Cowie, and Wang. Since FIRGs as a class cannot approach the x-ray fluxes of the centers of rich clusters, they must therefore be characterized in general by much smaller ratios of $L(\mathrm{x})/L(\mathrm{H}\alpha)$, and so their nebulae are not good cooling-flow candidates.

Another well-defined class of large extragalactic emission-line nebulae are those associated with the radio jets and lobes of some radio sources (cf. the recent review of van Breugel 1986). While the radio properties of our sample of FIRGs are largely unknown, the radio sources associated with Arp 220, NGC 6240, M82, and NGC 253 are weak and have little if any morphological similarity to the emission-line nebulae.

Finally, we consider the possibility that the FIRG nebulae are the direct result of a galaxy interaction. Fosbury and Wall (1979) first suggested that the LINER-type gas in NGC 6240 was simply the shock-heated interstellar media of two gas-rich colliding galaxies, while Harwit *et al.* (1986) have recently generalized this model to account for diverse properties of powerful FIRGs. The large emission-line nebulae associated with some quasars (Stockton and MacKenty 1983) and radio galaxies (e.g., Danziger *et al.* 1984) have been interpreted as gaseous tidal debris photoionized by an active nucleus. Our chief argument against these interpretations is essentially a morphological one: the very large 10 kpc scale "shell" or "bubble" structures in Arp 220 (simple) and NGC 6240 (complex), and the perpendicular orientation of the bright inner gas relative to the inner dust lane (Arp 220) and stellar disk (NGC 6240, M82, NGC 253), are difficult to understand in a galaxy collision/interaction model, but are natural in a wind model.

We conclude that while the evidence for a superwind origin for the emission-line gas in FIRGs is inconclusive, the alternatives are much less plausible.

d) Implications of A Wind Model

The quantitative details of the model described in Subsec. *b* above are discussed in MHvB in the context of the very well-studied tepid FIRG M82. Heckman *et al.* (1986) have applied a somewhat similar model to explain the excitation of the strong H_2 emission lines observed from the Seyfert galaxy NGC 7469 and other infrared-bright galaxies. Here, we limit our discussion of the implications of large-scale winds to a brief consideration of the scaling-up of a Chevalier and Clegg (1985) model to more powerful tepid FIRGs.

If we simply scale the estimated M82 supernova rate by the bolometric (mostly mid/far infrared) luminosity, we would expect that galaxies such as those in Table III are characterized by supernova rates of 3–30 per year. Using the estimates of Chevalier and Clegg, this implies that the winds carry a mass flux of up to ~ 10–$100\ M_\odot$/yr and a mechanical energy flux of up to $\sim 10^{44}$–10^{45} erg s^{-1}. If starbursts last for up to $\sim 10^8$ yr—as suggested by some models (e.g., Rieke *et al.* 1980, 1985)—then as much as $\sim 10^9$–$10^{10}\ M_\odot$ and 10^{60} erg of mechanical energy could be injected into the intergalactic medium by a "superstarburst" galaxy like Arp 220 or NGC 6240.

If this basic idea is correct and large-scale "superwinds" of highly enriched material are a characteristic feature of galaxies undergoing rapid star formation, it could have profound consequences for our understanding of galaxy formation (especially for the Ostriker and Cowie (1981) "explosions" theory), the chemical evolution of galaxies and the intergalactic medium, the nature of QSO absorption-line clouds, and a host of related topics.

To test the superwind model, we have begun a narrow-band (Hα) imaging survey of powerful FIRGs and plan a detailed investigation of the dynamical, physical, and chemical state of the best examples of bright emission-line nebulae associated with FIRGs. Clearly, a lot of exciting work lies ahead.

We would like to thank the staffs of KPNO and CTIO for their assistance in acquiring and reducing the data presented in these pages. We thank Colin Norman, Ralph Pudritz, and Roger Chevalier for stimulating discussions of starbursts and winds. The research of T.M.H. and L.A. is supported by NSF grant AST 85-15896, the Alfred P. Sloan Foundation, and NASA's *IRAS* Data Analysis Program (funded through the Jet Propulsion Laboratory).

REFERENCES

Armus, L., Heckman, T., and Miley, G. (1986). In preparation (AHM).

Baldwin, J. A., Phillips, M. M., and Terlevich, R. (1981). Publ. Astron. Soc. Pac. **93**, 5.

Binette, L., Dopita, M. A., and Tuohy, I. R. (1985). Astrophys. J. **297**, 476.

Chevalier, R. A., and Clegg, A. W. (1985). Nature **317**, 44.

Cutri, R. M., Rieke, G. H., and Lebofsky, M. J. (1984). Astrophys. J. **287**, 566.

Danziger, I. J., Fosbury, R. A. E., Goss, W. M., Bland, J., and Boksenberg, A. (1984). Mon. Not. R. Astron. Soc. **208**, 589.

DeGrijp, M. H. K., Miley, G. K., Lub, J., and de Jong, T. (1985). Nature **314**, 240.

de Jong, T., Clegg, P. E., Soifer, B. J., Rowan-Robinson, M., Habing, H. J., Houck, J. R., Aumann, H. H., and Raimond, E. (1984). Astrophys. J. Lett. **278**, L67.

DePoy, D. L., Becklin, E. E., and Wynn-Williams, G. (1986). Astrophys. J. **307**, 116.

Evans, I. N., and Dopita, M. A. (1985). Astrophys. J. Suppl. **58**, 125.

Fabian, A. C., Nulsen, P. E. J., and Canizares, C. R. (1984). Nature **310**, 733.

Fosbury, R. A. E., and Wall, J. V. (1979). Mon. Not. R. Astron. Soc. **189**, 79.

French, H. B. (1980). Astrophys. J. **240**, 41.

Fried, J. W., and Schulz, H. (1983). Astron. Astrophys. **118**, 166.

Gehrz, R. D., Sramek, R. A., and Weedman, D. W. (1983). Astrophys. J. **267**, 551.

Harwit, M., Houck, J. R., Soifer, B. T., and Palumbo, G. G. C. (1986). Preprint.

Heckman, T. M. (1986). Publ. Astron. Soc. Pac. **98**, 159.

Heckman, T. M., Balick, B., and Crane, P. C. (1980). Astron. Astrophys. Suppl. **40**, 285.

Heckman, T. M., Beckwith, S., Blitz, L., Skrutskie, M., and Wilson, A. S. (1986). Astrophys. J. **305**, 157.

Hu, E. M., Cowie, L. L., and Wang, Z. (1985). Astrophys. J. Suppl. **59**, 447.

Joseph, R. D., Wright, G. S., and Wade, R. (1984). Nature **311**, 132.

Keel, W. C. (1984). Astrophys. J. **282**, 75.

Koski, A. T. (1978). Astrophys. J. **223**, 56.

Landolt, A. U. (1973). Astron. J. **78**, 959.

Landolt, A. U. (1983). Astron. J. **88**, 439.

Lonsdale, C. J., Helou, G., Good, J. C., and Rice, W. (1985). *Cataloged Galaxies and Quasars Observed in the IRAS Survey* (Jet Propulsion Laboratory, Pasadena).

McCall, M. L., Rybski, P. M., and Shields, G. A. (1985). Astrophys. J.

Suppl. **57**, 1.
McCarthy, P., Heckman, T. M., and van Breugel, W. J. M. (1987). Astron. J. **93**, 264 (MHvB).
Miley, G. K., Neugebauer, G., and Soifer, B. T. (1985). Astrophys. J. Lett. **293**, L11.
Norris, R. P., Baan, W. A., Haschick, A. D., Diamond, P. J., and Booth, R. S. (1985). Mon. Not. R. Astron. Soc. **213**, 824.
Ostriker, J. P., and Cowie, L. L. (1981). Astrophys. J. Lett. **243**, L127.
Raymond, J. (1979). Astrophys. J. Suppl. **39**, 1.
Rieke, G. H., Cutri, R. M., Black, J. H., Kailey, W. F. McAlary, C. W., Lebofsky, M. J., and Elston, R. (1985). Astrophys. J. **290**, 116.
Rieke, G. H., and Lebofsky, M. J. (1986). Astrophys. J. **304**, 326.
Rieke, G. H., Lebofsky, M. J., Thompson, R. I., Low, F. J., and Tokunaga, A. T. (1980). Astrophys. J. **238**, 24.
Sarazin, C. L. (1986). Rev. Mod. Phys. **58**, 1.
Shull, J. M., and McKee, C. F. (1979). Astrophys. J. **227**, 131.
Soifer, B. T., *et al.* (1984). Astrophys. J. Lett. **278**, L71.
Stockton, A., and MacKenty, J. W. (1983). Nature **305**, 678.
Terlevich, R., and Melnick, J. (1985). Mon. Not. R. Astron. Soc. **213**, 841.
Toomre, A., and Toomre, J. (1972). Astrophys. J. **178**, 623.
van Breugel, W. J. M. (1986). Can. J. Phys. **64**, 392.
Watson, M. G., Stanger, V., and Griffiths, R. E. (1984). Astrophys. J. **286**, 144.

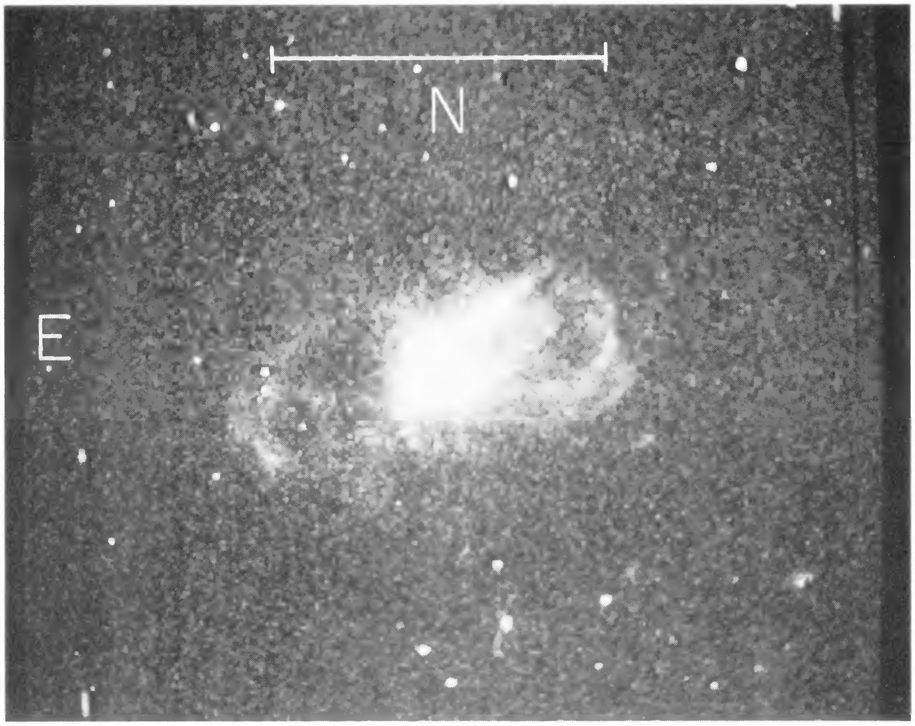

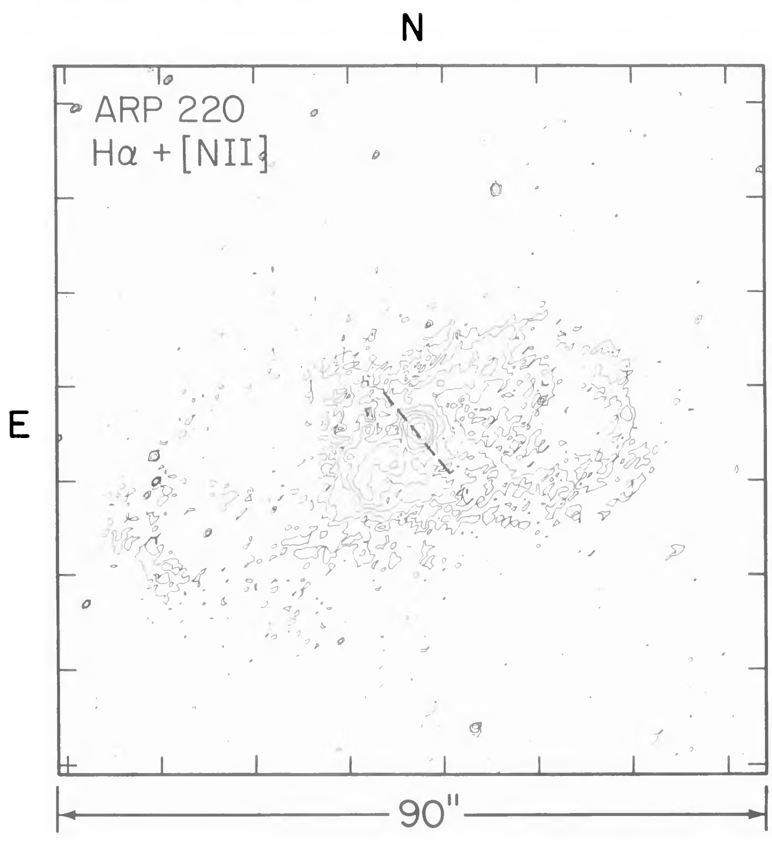

FIG. 2. (a) Narrowband image of Arp 220 taken in the light of redshifted Hα plus [N II] λλ 6548, 6584. The image shown represents pure emission-line light (the continuum was digitally subtracted using a suitably scaled broadband image). North is to the top and east to the left. The bar indicates a scale of 1 arcmin (= 21 kpc at Arp 220). (b) Contour plot of the Hα + [N II] image of Arp 220. The first contour is at a surface brightness of 3.4×10^{-17} erg cm^{-2} s^{-1} $arcsec^{-2}$, and each subsequent contour represents a factor of 2 higher surface brightness. The tick marks around the boundaries of the plot are separated by 12 arcsec. The dashed line represents the orientation of the central dust lane in Arp 220.

Heckman *et al.* (see page 277)

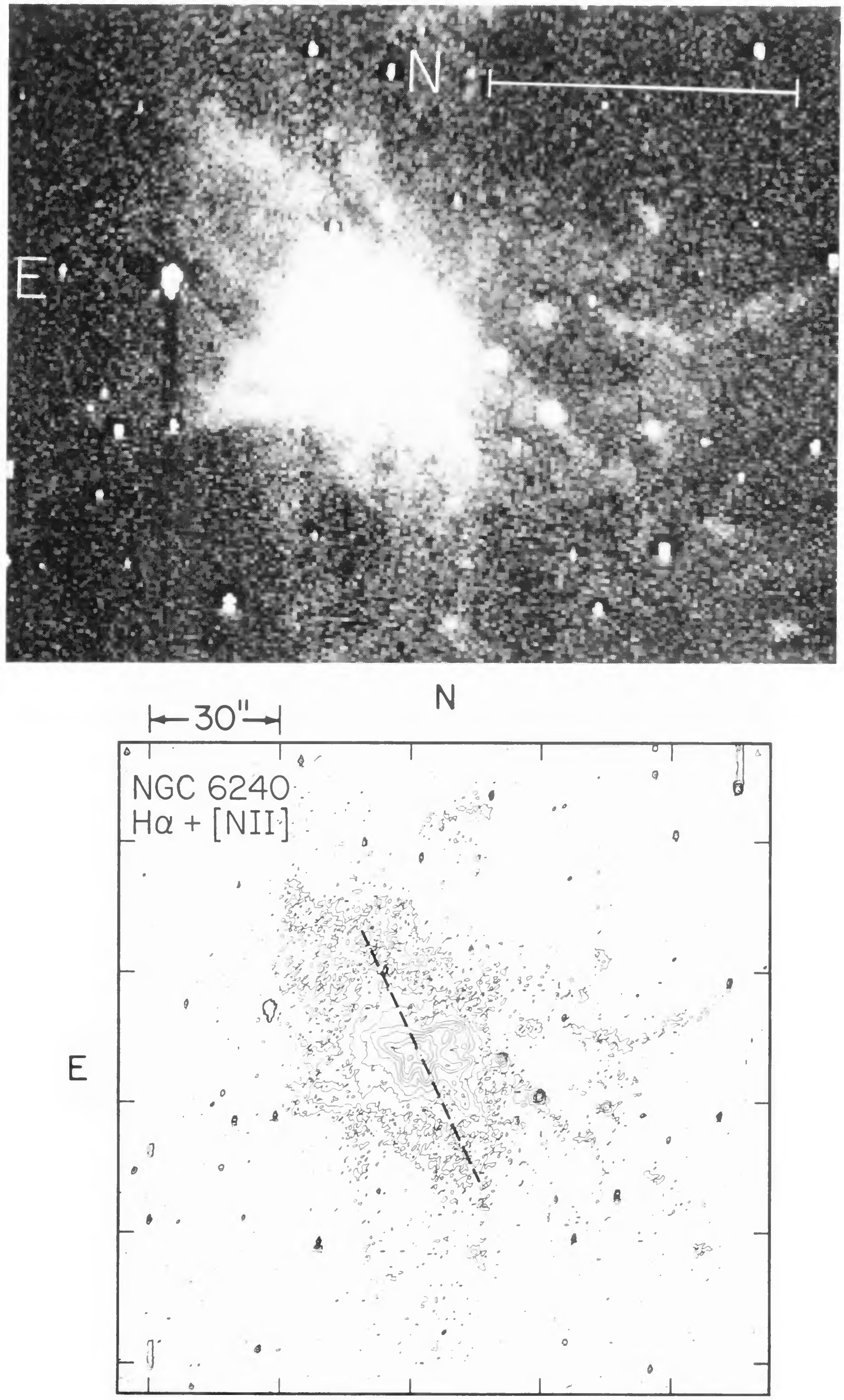

FIG. 3. (a) Narrowband image of NGC 6240 taken in the light of redshifted Hα plus [N II] λλ 6548, 6584. The continuum has been subtracted off using a suitably scaled broadband image. Scale and orientation are indicated as in Figs. 2(a) and (b) (1 arcmin = 28.5 kpc at NGC 6240). (b) Contour plot of the Hα + [N II] image of NGC 6240. The first contour is at a surface brightness of 6.6×10^{-17} erg cm^{-2} s^{-1} $arcsec^{-2}$ and each subsequent contour represents a factor of 2 higher surface brightness. The tick marks around the boundary of the plot are separated by 30 arcsec. The dashed line represents the orientation of the galaxy major axis.

Heckman *et al.* (see page 277)